Research Article

Kinematic Analysis of a Partially Decoupled 3-DOF Parallel Wrist

Fan Zhang,[1] Yunping Zhu,[1] Tomonari Furukawa,[2] and Wanqing Song[1]

[1]*Shanghai University of Engineering Science, Shanghai 24060, China*
[2]*Department of Mechanical Engineering, Virginia Tech, Blacksburg, VA 24060, USA*

Correspondence should be addressed to Fan Zhang; pdszhangfan@aliyun.com and Wanqing Song; swqls@126.com

Received 15 July 2015; Revised 7 October 2015; Accepted 22 October 2015

Academic Editor: Shahram Payandeh

A unique spherical parallel wrist with three partially decoupled rotational degrees of freedom (DOFs) is introduced in this paper. The mechanism has the significant advantages of few singularities and simple partially decoupled kinematics. A modified parallel wrist is optimized to have the least link interference workspace. Finally, the decoupled motion is studied in detail to exhibit the kinematic performance of the mechanism.

1. Introduction

Recent research focuses on the parallel wrist manipulators with two or three motorized axes [1–8]. The parallel wrist manipulators could be an effective tool for wrist, shoulder, and ankle instrument in medical robots, tracking mechanism, and advanced manufacturing mechanisms. To achieve high performance, including low inertia and high accuracy, remains challenging in the above mentioned fields, which gives rise to the study of the structural synthesis and optimization for the 3-DOF parallel wrist manipulators.

The coupled parallel wrist manipulators refer to the mechanisms whose input-output kinematics are nonlinear [9]. Existing researches revealed the problems about coupled parallel wrists, such as the singularities and the workspace problems. "Agile eye" is one of the most well-known parallel wrists, whose workspace is flawed with six singularity curves which correspond to self-motions of the moving-platform [10]. The Omni-Wrist III mechanism has a singularity-free workspace; however, the workspace is bounded by a spatial curved surface due to its variable center-of-rotation characteristic [11]. A family of 2-DOF coupled rotational parallel manipulators with an equal-diameter spherical pure rotation (ESPR) are proposed, to improve the workspace problem of Omni-Wrist [2]. Other coupled parallel wrists like the 3-RRUR [7], the 2-DOF 5R spherical parallel manipulator [5], the 3-UPU pure rotational parallel mechanism [6], the 2-DOF solar tracking mechanism [1], and the planar-spherical overconstrained mechanisms [12] are also reported to have the singularities or workspace problems.

The parallel wrists with diagonal matrix and triangular matrix are known as the partially decoupled parallel wrist (or the uncoupled parallel wrist) and the decoupled parallel wrist (or the fully decoupled parallel wrist), respectively. These mechanisms are reported to have fewer singularities and simple kinematics [13–15]. Carricato and Parenti-Castelli proposed a decoupled 2-DOF parallel wrist by optimizing the topology of mechanisms [14]. Hervé synthesized a family of 2-DOF parallel wrists which can achieve uncoupled pan-tilt motion by group theory method [15]. Zeng and Huang established the type synthesis method of the rotational decoupled parallel mechanism and proposed a novel 2-DOF decoupled parallel rotational wrist [16].

Though 2-DOF partially decoupled and decoupled parallel wrists have been well-studied, the methodology for kinematic analysis of the 3-DOF partially decoupled and decoupled parallel wrist still requires further investigations. Lubin et al. formulated the topology condition for the synthesis of the partially decoupled spherical parallel mechanism and obtained a novel 3-DOF partially decoupled spherical parallel mechanism [13]. Gogu presented a family of decoupled and partially decoupled 3-DOF parallel wrist [9]. Kuo and Dai

presented a fully decoupled remote center-of-motion parallel manipulator which can achieve 3-DOF spherical motion and a translational motion [17]; later they also proposed a variant of the Agile Eye with fully decoupled structure [18]. The methodology for the kinemaic analysis of partially decoupled wrists still needs further research to formulate a general method for 3-DOF spherical parallel wrists.

This paper proposed a unique partially decoupled 3-DOF parallel wrist. The fundamental of screw theory is briefly introduced in Section 2. The geometry of the parallel wrist is introduced in Section 3. And the link analysis is presented by using the reciprocal screw theory in Section 4. The singularity analysis is presented in Section 5. The kinematics analysis is presented in Section 6. And the workspace analysis and decoupled motion study are discussed in Sections 7 and 8. Finally, discussion and conclusion are addressed in Section 9.

2. The Fundamental of Screw Theory

2.1. The Reciprocal Screw Theory. A screw is six-dimensional in a homogeneous coordinate, which can completely describe the direction and position of vector in three-dimensional space. The reciprocal product of two screws $\$_1 = [\mathbf{s}_1, \mathbf{s}_1^0]$ and $\$_2 = [\mathbf{s}_2, \mathbf{s}_2^0]$ can be represented as [19]

$$\$_1 \circ \$_2 = \mathbf{s}_1 \cdot \mathbf{s}_2^0 + \mathbf{s}_2 \cdot \mathbf{s}_1^0. \tag{1}$$

The reciprocal product of two screws is equal to the instantaneous work of the wrench to the motion of the body:

$$\$_f \circ \$_m = \mathbf{f}_1 \cdot \mathbf{v}_2 + \mathbf{C}_1 \cdot \boldsymbol{\omega}_2 + a_{12}\mathbf{f}_1 \cdot \boldsymbol{\omega}_2, \tag{2}$$

where the twist $\$_m = [\boldsymbol{\omega}_2; \mathbf{r}_2 \times \boldsymbol{\omega}_2 + \mathbf{v}_2]$ denotes the instantaneous motion of the rigid body. The wrench $\$_f = [\mathbf{f}_1; \mathbf{r}_1 \times \mathbf{f}_1 + \mathbf{C}_0^1]$ denotes the wrench imposed on the rigid body.

If the reciprocal product is zero, the wrench denotes the constraint of the mechanical system to the instantaneous motion of rigid body. The geometrical conditions of the constraint and the instantaneous motion are as follows:

(i) If the constraint is a force, the force is perpendicular to the translational motion and is coplanar (intersecting, parallel, or coaxial) with the revolute motion.

(ii) If the constraint is a torque, the torque is perpendicular to the rotational motion.

2.2. The Constraint and Actuation Wrench of the Limb. The serial kinematic limb may be considered as a serial chain of C_i number of 1-DOF joints. The instantaneous motion of the moving-platform, $\$_p$, can be expressed as a linear combination of C_i twists [20],

$$\$_p = \sum_{i=1}^{C_j} \dot{\theta}_{i,j} \$_{i,j} \quad \text{for } j = 1, 2, \ldots F, \tag{3}$$

where $\dot{\theta}_{i,j}$ denotes the intensity and $\$_{i,j}$ represents a unit screw associated with the ith joint of the jth kinematic limb. F denotes the number of limbs of the parallel mechanism.

The constraints of the jth kinematic limb, $\$_j^r$, which are reciprocal to C_j number of twists of jth limb [21]

$$\$_j^r \circ \$_{i,j} = 0 \quad j = 1, 2, \ldots, C_i \tag{4}$$

forms a (6-C_j) reciprocal screw system.

If we lock the actuated joint of jth limb, the rank of the reciprocal screw system increases by 1. The additional reciprocal screws, denoted as $\$_j^a$, are reciprocal to all the passive joint screws of jth limb and impose work on $\$_{k,j}$, the actuated joint of jth limb (the kth joint of jth limb) [21],

$$\begin{aligned} &\$_j^a \circ \$_{i,j} = 0 \quad \text{for } i = 1, 2, \ldots, k-1,\ k+1, \ldots, C_j \\ &\$_j^a \circ \$_{k,j} \neq 0. \end{aligned} \tag{5}$$

Thus for a given mechanism, the constraint and actuated wrench could be calculated by (4) and (5).

2.3. The Jacobian Matrix in Screw Formulation. The actuation matrix of the parallel mechanism can be formulated as [21]

$$\mathbf{J}_c = \begin{bmatrix} \$_1^{r\mathbf{T}} \\ \$_2^{r\mathbf{T}} \\ \vdots \\ \$_F^{r\mathbf{T}} \end{bmatrix}. \tag{6}$$

The constraint matrix of the parallel mechanism can be formulated as

$$\mathbf{J}_a = \begin{bmatrix} \dfrac{\$_1^{a\mathbf{T}}}{\left(\$_1^{a\mathbf{T}} \$_{k,1}\right)} \\ \dfrac{\$_2^{a\mathbf{T}}}{\left(\$_2^{a\mathbf{T}} \$_{k,2}\right)} \\ \vdots \\ \dfrac{\$_F^{a\mathbf{T}}}{\left(\$_F^{a\mathbf{T}} \$_{k,F}\right)} \end{bmatrix}. \tag{7}$$

Each row of constraint Jacobian matrix represents a constraint imposed by limb. The rows of actuation Jacobian matrix represent the actuation acting by limbs.

3. The Geometry of a Parallel Wrist

The general geometry of the partially decoupled 3-DOF parallel wrist of is shown in Figure 1 (Figure 1(b) is kinematically equivalent to Figure 1(a)). The mechanism consists of a base-platform, a moving-platform, and three kinematic limbs. The nomenclature for the kinematic joint is as follows: R stands for revolute joint; R^N stands for revolute joint with an axis across the origin O; P stands for prismatic joint; and U stands for universal joint.

Since the universal joint is equvilent to two intersecting revolute joints, three kinematic limbs are also denoted as limb

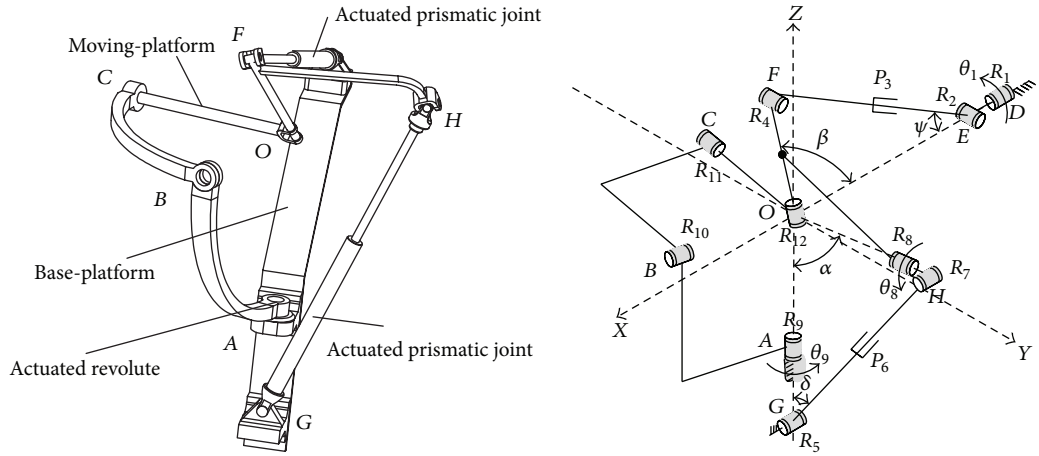

(a) The CAD model of partially decoupled parallel wrist (b) The schematic diagram of mechanism

Figure 1: The schematic diagram and design of the partially decoupled 3-DOF parallel wrist.

DEFO ($R_1{}^N R_2 P_3 R_4 R_{12}{}^N$), limb *GHO* ($R_5 P_6 R_7 R_8{}^N R_{12}{}^N$), and limb *ABCO* ($R_9{}^N R_{10}{}^N R_{11}{}^N$ limb), as shown in Figure 1(b). And $R_1{}^N \perp R_2$, $R_2 \perp P_3$, $R_2 // R_4 // R_8{}^N$, $R_5 \perp P_6$, $R_1 // R_5 // R_7$, $P_3 \perp P_6$, $R_9{}^N \perp R_{10}{}^N$, and $R_{10}{}^N \perp R_{11}{}^N$, while $\perp$ denotes lines are perpendicular, and // denotes lines are parallel in geometry. The actuated joints of the parallel wrist are prismatic joints P_6, P_3 and the revolute joint R_9. The moving-platform is attached at the link *CO*.

4. Limb Kinematics Analysis

A coordinate system *O-XYZ* is attached to the base-platform. The point *O* is chosen as the origin point; the *x*-axis is along the link *DE*, the *z*-axis is along the link *AO*, and the *y*-axis is perpendicular to both *x* and *z* axes.

Nomenclature used in this paper is as listed:

(i) $[X]^k$ denotes the posture of link *X* under the *O-XYZ* coordinate system, as a part of the *k* kinematic limb.

(ii) $[\mathbf{a}_i]^k$ denotes the axis of the revolute joint R_i under the *O-XYZ* coordinate system, as a part of the *k* kinematic limb.

(iii) θ_i denotes the rotated angle of the revolute joint R_i.

(iv) L_3 and L_6 denote the length of the actuated prismatic joints P_3 and P_6, respectively.

And the geometrics of the mechanism are defined as $OE = OG = a$, $OF = OH = b$, $L_3 = EF$, and $L_6 = GH$. And

$$\begin{aligned}
\beta &= \angle EOF = \arccos \frac{a^2 + b^2 - {L_3}^2}{2ab}, \\
\alpha &= \angle GOH = \arccos \frac{a^2 + b^2 - {L_6}^2}{2ab}, \\
\psi &= \angle OEF = \arccos \frac{a^2 + {L_3}^2 - b^2}{2aL_3}, \\
\delta &= \angle OGH = \arccos \frac{a^2 + {L_6}^2 - b^2}{2aL_6}.
\end{aligned} \tag{8}$$

$\mathrm{Rot}(\mathbf{a_i}, \theta_i)$ denotes the rotation matrix about the direction vector $\mathbf{a_i}$ by the angle θ_i and can be represented as [22]:

$$\begin{aligned}
&\mathrm{Rot}\left(\mathbf{a}_\mathbf{i}, \theta_i\right) \\
&= \begin{bmatrix}
a_x a_x \mathrm{vers}\,\theta_i + c\theta_i & a_y a_x \mathrm{vers}\,\theta_i - a_z s\theta_i & a_z a_x \mathrm{vers}\,\theta_i + a_y s\theta_i \\
a_x a_y \mathrm{vers}\,\theta_i + a_z s\theta_i & a_y a_y \mathrm{vers}\,\theta_i + c\theta_i & a_z a_y \mathrm{vers}\,\theta_i - a_x s\theta_i \\
a_x a_z \mathrm{vers}\,\theta_i - a_y s\theta_i & a_y a_z \mathrm{vers}\,\theta_i + a_x s\theta_i & a_z a_z \mathrm{vers}\,\theta_i + c\theta_i
\end{bmatrix},
\end{aligned} \tag{9}$$

where $\mathrm{vers}\,\theta_i = 1 - \cos\theta_i$, $c\theta_i = \cos\theta_i$, $s\theta_i = \sin\theta_i$, and $\mathbf{a_i} = \{a_x, a_y, a_z\}$.

By using formula (9), the axis of the *j*th kinematic joint of serial limb could be obtained,

$$\mathbf{a_j} = \mathrm{Rot}\left(\mathbf{a}_{j-1}, \theta_{i-1}\right) \cdots \mathrm{Rot}\left(\mathbf{a}_2, \theta_2\right) \mathrm{Rot}\left(\mathbf{a}_1, \theta_1\right). \tag{10}$$

4.1. DEFO Limb. The twist system of kinematic limb *DEFO* ($R_1{}^N R_2 P_3 R_4 R_{12}{}^N$) can be represented as

$$\begin{aligned}
\$_1 &= [1, 0, 0; 0, 0, 0] \\
\$_2 &= [0, \cos\theta_1, \sin\theta_1; 0, -\sin\theta_1, \cos\theta_1] \\
\$_3 &= [0, 0, 0; \cos\psi, -\sin\theta_1 \sin\psi, \cos\theta_1 \sin\psi] \\
\$_4 &= [0, \cos\theta_1, \sin\theta_1; \sin\beta, -\cos\beta \sin\theta_1, \cos\beta \cos\theta_1] \\
\$_{12} &= [-\cos\beta, -\sin\beta \sin\theta_1, \sin\beta \cos\theta_1; 0, 0, 0].
\end{aligned} \tag{11}$$

The constraint wrench system which the kinematic limb *DEFO* enforces on the moving-platform *CO* can be calculated by reciprocal screw theory:

$$\$^{\mathbf{r}}_{DEFO} = [0, \cos\theta_1, \sin\theta_1; 0, 0, 0]. \tag{12}$$

The constraint wrench $\$^{\mathbf{r}}_{DEFO}$ is the force which is across the origin and is parallel to the revolute joint R_2. The constraint wrench $\$^{\mathbf{r}}_{DEFO}$ is along with the axis of revolute joint ${R_8}^N$, since the revolute joint ${R_8}^N$ is parallel to R_2.

Locking the actuation joint P_3, the actuation wrench of limb *DEFO* can be obtained by (5) as

$$\begin{aligned} &\$^a_{DEFO} \cdot \$_3 \neq 0 \\ &\$^a_{DEFO} \cdot \$_i = 0 \quad (i = 1, 2, 4, 12). \end{aligned} \tag{13}$$

Further,

$$\begin{aligned} &\$^a_{DEFO} \cdot \mathbf{v}_3 \neq 0 \\ &\$^a_{DEFO} \cdot \boldsymbol{\omega}_i = 0 \quad (i = 1, 2, 4, 12), \end{aligned} \tag{14}$$

where $\boldsymbol{\omega}_i$ denotes the angle velocity of the revolute joints R_i $(i = 1, 2, 4, 12)$ and $\mathbf{v}_3$ denotes the velocity of the prismatic joint P_3.

The actuation wrench of limb *DEFO*, which is the force along with the axis of the prismatic joint P_3, is obtained by (14) as

$$\$^a_{DEFO} = [\cos\psi, -\sin\theta_1 \sin\psi, \cos\theta_1 \sin\psi; 0, 0, 0]. \tag{15}$$

4.2. GHO Limb. The twist system of kinematic limb *GHO* can be represented as

$$\begin{aligned} \$_5 &= [1, 0, 0; 0, 1, 0] \\ \$_6 &= [0, 0, 0; 0, \sin\delta, \cos\delta] \\ \$_7 &= [1, 0, 0; 0, \cos\alpha, \sin\alpha] \\ \$_8 &= [0, \sin\alpha, -\cos\alpha; 0, 0, 0] \\ \$_{12} &= [\sin\theta_8, \cos\alpha\cos\theta_8, \sin\alpha\cos\theta_8; 0, 0, 0]. \end{aligned} \tag{16}$$

The constraint wrench system which the kinematic limb *GHO* enforces on the moving-platform *CO* can be calculated as

$$\$^{\mathbf{r}}_{GHO} = [1, 0, 0; 0, 0, 0]. \tag{17}$$

The constraint wrench $\$^{\mathbf{r}}_{GHO}$ is the force along the x-axis.

Locking the actuation joint P_6, the actuation wrench of kinematic limb *GHO* can be obtained by

$$\begin{aligned} &\$^a_{DEFO} \cdot \mathbf{v}_6 \neq 0 \\ &\$^a_{DEFO} \cdot \boldsymbol{\omega}_i = 0 \quad (i = 5, 7, 8, 12). \end{aligned} \tag{18}$$

The actuation wrench of limb *GHO*, which is the force along with the axis of the prismatic joint P_3, is obtained by (18) as

$$\$^a_{GHO} = [0, \sin\delta, \cos\delta; 0, 0, 0]. \tag{19}$$

4.3. ABCO Limb. The twist system of kinematic limb *ABCO* can be represented as

$$\begin{aligned} \$_9 &= [0, 0, -1; 0, 0, 0] \\ \$_{10} &= [a_{10}, b_{10}, c_{10}; 0, 0, 0] \\ \$_{11} &= [a_{11}, b_{11}, c_{11}; 0, 0, 0]. \end{aligned} \tag{20}$$

The constraint wrench system which the kinematic limb *ABCO* enforces on the moving-platform *CO* and can be calculated as

$$\begin{aligned} \$^{\mathbf{r}}_{1,ABCO} &= [1, 0, 0; 0, 0, 0] \\ \$^{\mathbf{r}}_{2,ABCO} &= [0, 1, 0; 0, 0, 0] \\ \$^{\mathbf{r}}_{3,ABCO} &= [0, 0, 1; 0, 0, 0]. \end{aligned} \tag{21}$$

The constraint wrench system consists of three nonlinear forces $\$^{\mathbf{r}}_{1,ABCO}$, $\$^{\mathbf{r}}_{2,ABCO}$, and $\$^{\mathbf{r}}_{3,ABCO}$, which intersect at the origin point.

Locking the actuation joint R_9, the actuation wrench of limb *ABCO*, which is a torque along with the z-axis, can be obtained as

$$\$^a_{ABCO} = [0, 0, 0; 0, 0, 1]. \tag{22}$$

5. Singularity Analysis

The Jacobian matrix of parallel mechanism can be represented as the actuation Jacobian matrix and constraint Jacobian matrix [21]. Thus the singularities occur: (i) when the actuation Jacobian matrix is singular, while the constraint Jacobian matrix is invertible; (ii) when the constraint Jacobian matrix is singular; (iii) when the kinematic limb is singular [21, 23].

When the matrix A is singular, that means the row vectors of the matrix are linear. In this way, the singular problem of Jacobian matrix can be transformed into judging the ranks of the wrench system and twist system of limbs.

5.1. The Constraint Singularity. The constraint wrench system of moving-platform is determined by (12), (17), and (21),

$$\begin{aligned} \$^{\mathbf{r}}_{GHO} &= [1, 0, 0; 0, 0, 0] \\ \$^{\mathbf{r}}_{DEFO} &= [0, \cos\theta_1, \sin\theta_1; 0, 0, 0] \\ \$^{\mathbf{r}}_{1,ABCO} &= [1, 0, 0; 0, 0, 0] \\ \$^{\mathbf{r}}_{2,ABCO} &= [0, 1, 0; 0, 0, 0] \\ \$^{\mathbf{r}}_{3,ABCO} &= [0, 0, 1; 0, 0, 0]. \end{aligned} \tag{23}$$

It is easy to see that the rank of the constraint wrench systems keeps 3, which means the constraint Jacobian matrix will be nonsingular. This parallel wrist has no constrain singularities across the workspace.

The DOF of the parallel wrist can be verified by these constraints. Based on the reciprocal screw theory, the twist system of the moving-platform can be calculated,

$$\begin{aligned}\$_1^{\mathbf{m}} &= [1,0,0;0,0,0]\\ \$_2^{\mathbf{m}} &= [0,1,0;0,0,0]\\ \$_3^{\mathbf{m}} &= [0,0,1;0,0,0]\,.\end{aligned} \tag{24}$$

As seen from (24), the parallel wrist has three successive rotational DOFs, which guarantee the moving-platform of the parallel wrist can achieve the spherical motion around the origin.

5.2. The Actuation Wrench Singularity. The actuation wrench system of moving-platform is determined by (15), (19), and (22),

$$\begin{aligned}\$_{DEFO}^{a} &= [\cos\psi, -\sin\theta_1\sin\psi, \cos\theta_1\sin\psi; 0,0,0]\\ \$_{GHO}^{a} &= [0, \sin\delta, \cos\delta; 0,0,0]\\ \$_{ABCO}^{a} &= [0,0,0;0,0,1]\,.\end{aligned} \tag{25}$$

The forces $\$_{DEFO}^{a}$ and $\$_{GHO}^{a}$ keep nonlinear. The torque $\$_{a}^{ABCO}$ is nonlinear with both $\$_{DEFO}^{a}$ and $\$_{GHO}^{a}$. Since the rank of actuation wrench system does not decrease, the actuation Jacobian matrix will be invertible. The parallel wrist has no actuation singularities across the workspace.

5.3. The Limb Singularity. Limb singularities occur at the following configurations:

(i) When $\beta = 0^\circ$ or $\beta = 180^\circ$, $\$_1$ and $\$_{12}$ are linear and the actuation joint P_3 will be locked by the mechanical system; the rank of twist system of limb *DEFO* will decrease to 1.

(ii) When $\alpha = 0^\circ$ or $\alpha = 180^\circ$, the actuation joint P_6 will be locked by the mechanical system; the rank of twist system of limb *GHO* will decrease to 2.

(iii) When the angle of revolute joint R_{10} is zero, that means the limb *ABCO* is folded; the rank of twist system of the limb *ABCO* will decrease to 2.

Under these configurations, the DOFs of the kinematic limb will degenerate, the parallel mechanism will fail to meet the condition of three rotational DOFs, and the mechanism will be locked.

6. Kinematics Analysis

6.1. Inverse Kinematics. The output angles and input values of the parallel wrist are the angles $\theta_1, \theta_8, \theta_{12}$ and L_6, L_3, θ_9, respectively. Usually the inverse kinematics of parallel mechanism can be accomplished by the rotation matrix [24] or kinematics modeling [25]. However, for the partially decoupled parallel wrist, the inverse kinematics can be further derived to two linear and one nonlinear kinematic equations.

6.1.1. The Input Value of the Active Prismatic Joints. Since the angle α is defined as the angle between the links *OG* and *OH*, β is defined as the angle between the links *OE* and *OF*; the relationships between α, β and θ_1, θ_8 can be observed as $\alpha = \theta_1 + \pi/2$, $\beta = \theta_8 + \pi/2$.

The input value of the active prismatic joints can be obtained from the geometrics of the triangles $\triangle EOF$ and $\triangle GOH$,

$$\begin{aligned}L_3 &= \sqrt{a^2 + b^2 - 2ab\cos\beta}\\ L_6 &= \sqrt{a^2 + b^2 - 2ab\cos\alpha}.\end{aligned} \tag{26}$$

6.1.2. The Input Value of the Active Revolute Joint. According to the topology of the parallel wrist, the revolute joints R_{11} and R_{10} are perpendicular. Hence, the dot product of the axis vectors of revolute joints R_{11} and R_{10} should be zero:

$$[\mathbf{a}_{11}]^{DEFO} \cdot [\mathbf{a}_{10}]^{ABCO} = 0. \tag{27}$$

Substituting the coordinates of $\mathbf{a}_{11}$ in (11) and $\mathbf{a}_{10}$ in (20) and into (27), we obtain

$$\theta_9 = \arctan\frac{\sin\theta_{12}\sin\beta}{\cos\theta_{12}\cos\theta_1 + \sin\theta_{12}\cos\beta\sin\theta_1}, \tag{28}$$

where $\cos\theta_{12}\cos\theta_1 + \sin\theta_{12}\cos\beta\sin\theta_1 \neq 0$.

Finally the inverse kinematics of the mechanism can be obtained from (26) and (28),

$$\begin{aligned}L_3 &= \sqrt{a^2 + b^2 + 2ab\sin\theta_8}\\ L_6 &= \sqrt{a^2 + b^2 + 2ab\sin\theta_1}\\ \theta_9 &= \arctan\frac{\sin\theta_{12}\sin\beta}{\cos\theta_{12}\cos\theta_1 + \sin\theta_{12}\cos\beta\sin\theta_1}.\end{aligned} \tag{29}$$

6.2. Direct Kinematics. The direct kinematic problem was solved by establishing the kinematics constraint equations of the same link under different kinematic limbs. The first two output angles were derived by formulating the kinematics of the link *OF*; then the third output angle was obtained by the kinematics of the moving-platform *CO*.

6.2.1. The Two Decoupled Output Angles of Moving-Platform. The posture of revolute joint R_{12} associated with the different kinematic limbs should be the same. Thus, the vector of the axis of R_{12} in (11) and (16) should be the equivalent, obtaining

$$[\mathbf{a}_{12}]^{DEFO} = [\mathbf{a}_{12}]^{GHO}. \tag{30}$$

Further we yields

$$\begin{bmatrix} -\cos\beta \\ -\sin\beta\sin\theta_1 \\ \sin\beta\cos\theta_1 \end{bmatrix} = \begin{bmatrix} \sin\theta_8 \\ \cos\alpha\cos\theta_8 \\ \sin a\cos\theta_8 \end{bmatrix}. \tag{31}$$

The output angle of the moving-platform, θ_1 and θ_8, can be calculated as

$$\theta_1 = \alpha - \frac{\pi}{2}$$
$$\theta_8 = \beta - \frac{\pi}{2}. \tag{32}$$

6.2.2. The Third Coupled Output Angle of Moving-Platform. Based on the derived equation (27), the output angle θ_{12} can be obtained:

$$\theta_{12} = \arctan \frac{\cos\theta_1 \sin\theta_9}{\cos\theta_9 \sin\beta - \cos\beta \sin\theta_1 \sin\theta_9} \tag{33}$$

while $\cos\theta_9 \sin\beta - \cos\beta \sin\theta_1 \sin\theta_9 \neq 0$.

Combining (32) and (33), the direct kinematics of the moving-platform CO are obtained:

$$\theta_1 = \alpha - \frac{\pi}{2} \tag{34}$$

$$\theta_8 = \beta - \frac{\pi}{2} \tag{35}$$

$$\theta_{12} = \arctan \frac{\cos\theta_1 \sin\theta_9}{\cos\theta_9 \sin\beta - \cos\beta \sin\theta_1 \sin\theta_9}. \tag{36}$$

Among the three DOFs of parallel wrist, two rotational DOFs are independent DOFs, and each DOF is controlled by a single actuated joint. The third rotational DOF around R_{12} is actuated by prismatic joints P_6, P_3 and the revolute joint R_9. The parallel wrist is a partially decoupled mechanism.

7. Workspace Analysis

The wrist mechanism has three rotational DOFs, so the workspace is defined as all reachable positions of the platform about a fixed point in 3D space. There are three main mechanical constraints that limit the workspace of the parallel wrist: (i) the actuators' stroke, (ii) the range of the passive joints, and (iii) the link interference. By applying the inverse kinematics of parallel wrist, we judge the boundaries of the orientation workspace.

(i) The Actuators' Stroke. Consider

$$L_{6\min} \leq L_6 \leq L_{6\max},$$
$$L_{3\min} \leq L_3 \leq L_{3\max}, \tag{37}$$

where $L_{6\min}$ and $L_{6\max}$ are, respectively, the minimum and maximum lengths of prismatic joints L_6 and where $L_{3\min}$ and $L_{3\max}$ are, respectively, the minimum and maximum lengths of prismatic joints L_3. When L_6 is equal to $L_{6\min}$ or $L_{6\max}$, L_3 is equal to $L_{3\max}$ or $L_{3\min}$; the node can be written into the array which forms the boundary of the orientation workspace.

(ii) Range of the Passive Joints. The universal joints in the mechanism are replaced by two intersecting joints, and the range of the passive revolute joints could be considered to be $(0, 2\pi]$. Thus during the calculation of the workspace, the range of the passive joints is ignored.

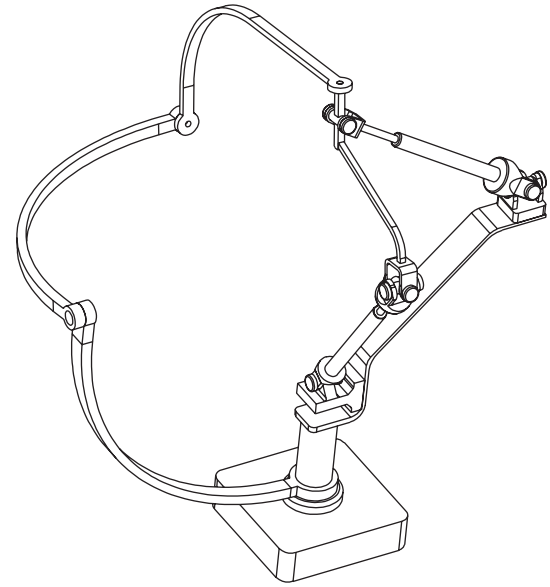

Figure 2: The modified parallel wrist.

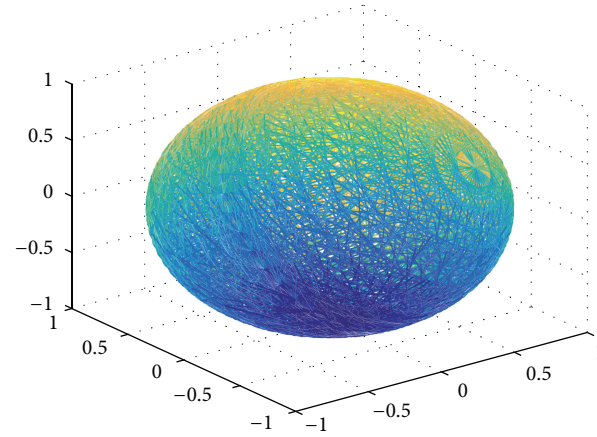

Figure 3: The workspace of the parallel wrist.

(iii) Link Interference. The links of parallel wrist can be approximated by cylinders of diameter D. The minimum distance between every two adjacent line segments is D_i. The constraint on the relative position of all pairs of links can be denoted as

$$D_i \geq D. \tag{38}$$

The minimum distance between two line segments can be calculated by the multistep algorithm introduced in [26].

Based on the least interference design methodology introduced in [27], the parallel wrist is optimized to have the maximum link interference-free workspace, as shown in Figure 2. There is only quite little link interference between links OF and FE, when the triangle $\triangle EOF$ degenerates to the coaxial lines.

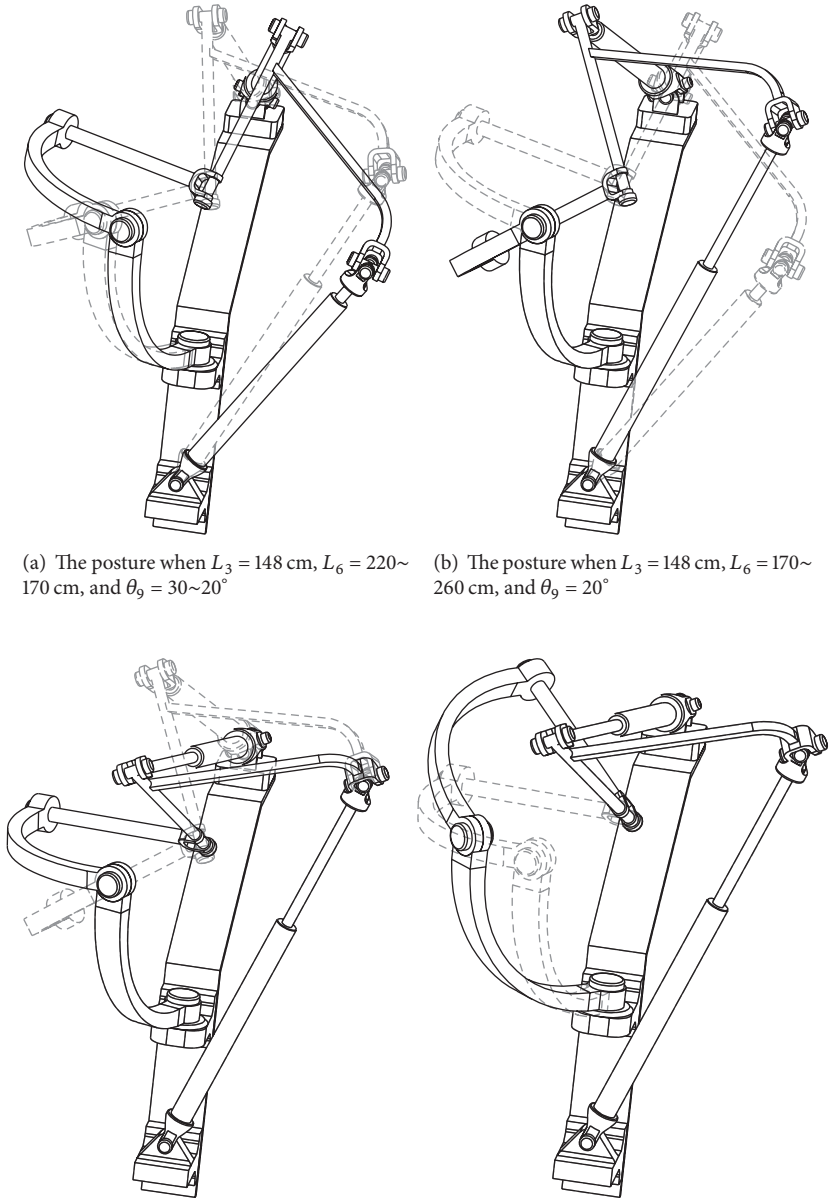

(a) The posture when $L_3 = 148$ cm, $L_6 = 220\sim 170$ cm, and $\theta_9 = 30\sim 20^\circ$

(b) The posture when $L_3 = 148$ cm, $L_6 = 170\sim 260$ cm, and $\theta_9 = 20^\circ$

(c) The posture when $L_3 = 148\sim 258$ cm, $L_6 = 260$ cm, and $\theta_9 = 20^\circ$

(d) The posture when $L_3 = 258$ cm, $L_6 = 260$, and $\theta_9 = 20\sim 45^\circ$

Figure 4: The demonstration of partially decoupled motion.

The workspace analysis shows the workspace of the unit length vector associated with the moving-platform OC of the modified parallel wrist.

From Figure 3, we can derive the following:

(1) The output angle θ_1 of the parallel wrist is reachable within $(-\pi/2, \pi/2)$, when output angle θ_8 is equal to any angle within $(-\pi/2, \pi/2)$.

(2) The maximum range of output angle θ_8 can be $(0, 2\pi)$, which is optimized by on the least interference design methodology introduced in [27].

8. Decoupled Motion Study

The mathematical results of the cases are shown in Table 1. The results were developed by using the MATHEMATICA software package. The geometric parameters of the parallel wrist are given as $OE = OG = 200$ cm, $OF = OH = 100$ cm, and $OA = OB = OC = 98$ cm.

The performance of partially decoupled motion of the 3-DOF parallel wrist is shown in Figure 4. Four videos are attached as supplement materials (see Supplementary Material available online at http://dx.doi.org/10.1155/2015/790414):

(1) As shown in Figure 4(a), the parallel wrist changes from the 1st posture to 2nd posture.

Table 1: The cases of direct kinematics.

Posture	Input			Output		
	L_3 (cm)	L_6 (cm)	θ_9 (°)	θ_1 (°)	θ_8 (°)	θ_{12} (°)
1	148	220	30	45.23	−44.62	41.84
2	148	170	20	−31.84	−44.62	22.15
3	148	260	20	26.10	−44.62	22.30
4	258	260	20	26.10	24.46	11.23
5	258	260	45	26.10	24.46	24.26

The parallel wrist changes from the 1st posture (L_3 = 148 cm, L_6 = 220 cm, and $\theta_9 = 30^\circ$) to 2nd posture (L_3 = 148 cm, L_6 = 170 cm, and $\theta_9 = 20^\circ$). The output angle θ_8 stays at -44.62°. In Figure 4(a), the 1st posture is shown in dotted line, and the 2nd posture is shown in real line.

(2) As shown in Figure 4(b), the parallel wrist changes from the 2nd posture to the 3rd posture.

The parallel wrist changes from the 2nd posture (L_3 = 148 cm, L_6 = 170 cm, and $\theta_9 = 20^\circ$) to 3rd posture (L_3 = 148 cm, L_6 = 260 cm, and $\theta_9 = 20^\circ$). In Figure 4(b), the 2nd posture is shown in dotted line, and the 3rd posture is shown in real line.

(3) As shown in Figure 4(c), the parallel wrist changes from the 3rd posture to the 4th posture.

The parallel wrist changes from the 3rd posture (L_3 = 148 cm, L_6 = 260 cm, and $\theta_9 = 20^\circ$) to 4th posture (L_3 = 258 cm, L_6 = 260 cm, and $\theta_9 = 20^\circ$). In Figure 4(c), the 3rd posture is shown in dotted line, and the 4th posture is shown in real line.

(4) As shown in Figure 4(d), the parallel wrist changes from the 4th posture to the 5th posture.

The parallel wrist changes from the 4th posture (L_3 = 258 cm, L_6 = 260 cm, and $\theta_9 = 20^\circ$) to 5th posture (L_3 = 258 cm, L_6 = 260 cm, and $\theta_9 = 45^\circ$). In Figure 4(d), the 4th posture is shown in dotted line, and the 5th posture is shown in real line.

(5) As shown in Figures 4(a) and 4(b), output angle θ_8 is controlled by actuated joint P_3.

(6) As shown in Figures 4(c) and 4(d), output angle θ_1 is controlled by actuated joint P_6.

(7) As shown in Figures 4(b) and 4(c), output angle θ_{12} is controlled by actuated joints P_3, P_6, and R_9.

9. Conclusion and Discussion

In this paper, a 3-DOF spherical parallel wrist was introduced. Then link analysis is presented by using the reciprocal screw theory. As a result, the singularity analysis is deduced. The kinematics analysis and workspace analysis are presented. The decoupled motion analysis shows that the two rotational DOFs of the mechanism can be controlled by a single actuation, respectively, while the third rotational DOF is controlled by three actuated joints. Thus, the third DOF is a weak-coupling with the other two rotational DOFs.

The mechanism has linear kinematics, so it has the potential for application as the ankle or wrist of the robot. The kinematics of the parallel wrist is simple and easy to control, which ensures that the wrist will achieve high precision motion.

Conflict of Interests

The authors declare that there is no conflict of interests regarding the publication of this paper.

Acknowledgments

The authors would like to gratefully acknowledge the financial support from the National Natural Science Foundation of China (Grant no. 50975046) and Shanghai Nature Fund (Grant no. 14ZR1418500).

References

[1] A. Cammarata, "Optimized design of a large-workspace 2-DOF parallel robot for solar tracking systems," *Mechanism and Machine Theory*, vol. 83, pp. 175–186, 2015.

[2] K. Wu, J. Yu, G. Zong, and X. Kong, "A Family of rotational parallel manipulators with equal-diameter spherical pure rotation," *Journal of Mechanisms and Robotics*, vol. 6, no. 1, Article ID 011008, 2013.

[3] B. M. Schena, "Robotic arm with five-bar spherical linkage," Google Patents, 2013.

[4] J. S. Dai, M. Zoppi, and X. Kong, *Advances in Reconfigurable Mechanisms and Robots I*, Springer, 2012.

[5] X. Kong, "Forward displacement analysis and singularity analysis of a special 2-Dof 5r spherical parallel manipulator," *Journal of Mechanisms and Robotics*, vol. 3, no. 2, Article ID 024501, 2011.

[6] S. Huda, Y. Takeda, and S. Hanagasaki, "Kinematic design of 3-URU pure rotational parallel mechanism to perform precise motion within a large workspace," *Meccanica*, vol. 46, no. 1, pp. 89–100, 2011.

[7] R. Deidda, A. Mariani, and M. Ruggiu, "On the kinematics of the 3-RRUR spherical parallel manipulator," *Robotica*, vol. 28, no. 6, pp. 821–832, 2010.

[8] D. Gan, L. Seneviratne, and J. Dias, "Design and analytical kinematics of a robot wrist based on a parallel mechanism," in *Proceedings of the World Automation Congress (WAC '12)*, pp. 1–6, Puerto Vallarta, Mexico, June 2012.

[9] G. Gogu, *Structural Synthesis of Parallel Robots, Part 4: Other Topologies with Two and Three Degrees of Freedom*, vol. 183 of *Solid Mechanics and Its Applications*, Springer, Dordrecht, The Netherlands, 2012.

[10] I. A. Bonev, D. Chablat, and P. Wenger, "Working and assembly modes of the agile eye," in *Proceedings of the IEEE International Conference on Robotics and Automation (ICRA '96)*, pp. 2317–2322, Orlando, Fla, USA, 1996.

[11] J. Sofka, V. Skormin, V. V. Nikulin, and D. J. Nicholson, "Omni-Wrist III—a new generation of pointing devices. Part I. Laser beam steering devices—mathematical modeling," *IEEE Transactions on Aerospace and Electronic Systems*, vol. 42, no. 2, pp. 718–725, 2006.

[12] G. Wei and J. S. Dai, "Origami-inspired integrated planar-spherical overconstrained mechanisms," *Journal of Mechanical*

Design—Transactions of the ASME, vol. 136, no. 5, Article ID 051003, 2014.

[13] H. Lubin, W. Yan, and W. Jun, "Study on the decoupling conditions of the spherical parallel mechanism based on the criterion for topologically decoupled parallel mechanisms," *Chinese Journal of Mechanical Engineering*, vol. 41, no. 9, p. 28, 2005.

[14] M. Carricato and V. Parenti-Castelli, "A novel fully decoupled two-degrees-of-freedom parallel wrist," *The International Journal of Robotics Research*, vol. 23, no. 6, pp. 661–667, 2004.

[15] J. M. Hervé, "Uncoupled actuation of pan-tilt wrists," *IEEE Transactions on Robotics*, vol. 22, no. 1, pp. 56–64, 2006.

[16] D. Zeng and Z. Huang, "Type synthesis of the rotational decoupled parallel mechanism based on screw theory," *Science China Technological Sciences*, vol. 54, no. 4, pp. 998–1004, 2011.

[17] C.-H. Kuo and J. S. Dai, "Kinematics of a fully-decoupled remote center-of-motion parallel manipulator for minimally invasive surgery," *Journal of Medical Devices*, vol. 6, no. 2, Article ID 021008, 2012.

[18] C.-H. Kuo, J. S. Dai, and G. Legnani, "A non-overconstrained variant of the Agile Eye with a special decoupled kinematics," *Robotica*, vol. 32, no. 6, pp. 889–905, 2014.

[19] Z. Huang, Q. Li, and H. Ding, *Theory of Parallel Mechanisms*, Springer, New York, NY, USA, 2012.

[20] M. G. Mohamed and J. Duffy, "A direct determination of the instantaneous kinematics of fully parallel robot manipulators," *Journal of Mechanisms, Transmissions, and Automation in Design*, vol. 107, no. 2, pp. 226–229, 1985.

[21] S. A. Joshi and L.-W. Tsai, "Jacobian analysis of limited-DOF parallel manipulators," in *Proceedings of the ASME International Design Engineering Technical Conferences and Computers and Information in Engineering Conference*, pp. 341–348, Montreal, Canada, September-October 2002.

[22] D. F. Rogers and J. A. Adams, *Mathematical Elements for Computer Graphics*, McGraw-Hill Higher Education, 2nd edition, 1989.

[23] X.-J. Liu and J. Wang, "Singularity of parallel mechanisms," in *Parallel Kinematics*, pp. 129–148, Springer, 2014.

[24] J.-P. Merlet, *Parallel Robots*, Springer, 2001.

[25] D. Gan, J. S. Dai, J. Dias, and L. Seneviratne, "Unified kinematics and singularity analysis of a metamorphic parallel mechanism with bifurcated motion," *Journal of Mechanisms and Robotics*, vol. 5, no. 3, Article ID 031004, 2013.

[26] J.-P. Merlet, "Determination of the orientation workspace of parallel manipulators," *Journal of Intelligent & Robotic Systems*, vol. 13, no. 2, pp. 143–160, 1995.

[27] Z. Tao and Q. An, "Interference analysis and workspace optimization of 3-RRR spherical parallel mechanism," *Mechanism and Machine Theory*, vol. 69, pp. 62–72, 2013.